

See discussions, stats, and author profiles for this publication at: <https://www.researchgate.net/publication/355505361>

Enhanced Summertime Surface Warming Effects of Long-Term Urbanization in a Humid Urban Agglomeration in China

Article in *Journal of Geophysical Research: Atmospheres* · November 2021

DOI: 10.1029/2021JD035009

CITATIONS

13

READS

333

8 authors, including:



Longfei Han

Hunan Normal University

39 PUBLICATIONS 953 CITATIONS

[SEE PROFILE](#)



Xiaojun Deng

Zhejiang University of Finance and Economics

40 PUBLICATIONS 1,246 CITATIONS

[SEE PROFILE](#)



Liu Yang

Hengyang Normal University

32 PUBLICATIONS 501 CITATIONS

[SEE PROFILE](#)



Mu Xiao

University of California, San Diego

26 PUBLICATIONS 1,541 CITATIONS

[SEE PROFILE](#)

JGR Atmospheres

RESEARCH ARTICLE

10.1029/2021JD035009

Key Points:

- Long-term urbanization-induced climate effects in Yangtze River Delta urban agglomeration region were examined based on analyzing observations and performing numerical simulations
- Warming effect of urbanization was enhanced in both the magnitude and affected area in the late stage of urbanization
- Altered energy partitioning between sensible and latent heat fluxes by urban expansion was the key factor of warming atmosphere

Supporting Information:

Supporting Information may be found in the online version of this article.

Correspondence to:

M. Xiao,
Mu.Xiao@asu.edu

Citation:

Han, L., Yu, X., Xu, Y., Deng, X., Yang, L., Li, Z., et al. (2021). Enhanced summertime surface warming effects of long-term urbanization in a humid urban agglomeration in China. *Journal of Geophysical Research: Atmospheres*, 126, e2021JD035009. <https://doi.org/10.1029/2021JD035009>

Received 4 APR 2021

Accepted 16 OCT 2021

Author Contributions:

Conceptualization: Longfei Han, Xiaoqin Yu, Zhongwu Li
Formal analysis: Longfei Han, Xiaojun Deng, Dianqing Lv, Mu Xiao
Funding acquisition: Longfei Han, Youpeng Xu
Investigation: Longfei Han, Xiaoqin Yu, Xiaojun Deng, Liu Yang
Methodology: Longfei Han
Software: Longfei Han
Supervision: Youpeng Xu
Validation: Longfei Han, Mu Xiao
Writing – original draft: Longfei Han
Writing – review & editing: Longfei Han, Mu Xiao

© 2021. American Geophysical Union.
All Rights Reserved.

Enhanced Summertime Surface Warming Effects of Long-Term Urbanization in a Humid Urban Agglomeration in China

Longfei Han¹ , Xiaoqin Yu¹, Youpeng Xu², Xiaojun Deng³, Liu Yang⁴, Zhongwu Li¹, Dianqing Lv^{5,1}, and Mu Xiao⁶ 

¹College of Geographic Science, Hunan Normal University, Changsha, China, ²School of Geographic and Oceanographic Science, Nanjing University, Nanjing, China, ³School of Economics, Zhejiang University of Finance and Economics, Hangzhou, China, ⁴College of City and Tourism, Hengyang Normal University, Hengyang, China, ⁵School of Chemical and Environmental Engineering, Jiangsu University of Technology, Changzhou, China, ⁶School of Sustainable Engineering and the Built Environment, Arizona State University, Tempe, AZ, USA

Abstract In this study, we examined the summertime climatic effects of urban expansion during 1990–2010 in the Yangtze River Delta (YRD) region by analyzing station observations and performing numerical simulations with the Weather Research and Forecast (WRF) model. Long-term observations showed that urban area experienced a larger increase in summertime 2-m air temperature than rural part during 1980–2018, and the influence of urbanization on the urban-rural contrast was greater in the late stage (after 2000) than the early stage (before 2000). We applied the WRF model incorporated with historical land surface cover data (year 1990, 2000, and 2010) to further evaluate the climatic effects of long-term urbanization. On average, urban expansion over 1990–2010 led to 0.75°C increase in daily average temperature (1.06°C in daily minimum and 0.45°C in daily maximum) during the summer. The summertime daily temperature range decreased by 0.61°C in urban environment during the same period. Compared to the warming effect of urbanization in the 1990s, both the magnitude and affected area have increased after the millennium. Also, urban expansion reduced moisture in low-level atmosphere, and this urban dry island (UDI) effect was enhanced in the late stage. Less moisture in the atmosphere offset heat stress index induced by the warming temperature. We also found that the partitioning of net radiation between sensible and latent heat was the key factor that controlled urban warming effect.

Plain Language Summary Urbanization is a long-term dynamic process, while the dynamic climatic effect of urbanization was seldom investigated. In this study, we used both long-term observations and simulations to examine the urban effect on summer climate in Yangtze River Delta. We found that urban daily average temperature increased by 0.75°C, and urban warming effect was greater in the late stage (after 2000) than the early stage (before 2000). Urbanization also caused air humidity loss, which made urban area drier and was known as urban dry island (UDI) effect. The change of heat stress was relatively small due to UDI effect. Urbanization resulted in increased sensible heat fluxes and reduced latent heat fluxes, which determined the urban warming effect. This study provides insights to understand warming air temperature in humid urban agglomeration.

1. Introduction

Urbanization is one of the most dramatic characteristics of human activities over the past decades. Approximately one-third of the world's population reside in cities in 1950, and that number rises to 54% in 2014 (AAAS, 2016). It is estimated that the percentage will reach 66% in 2050 (McDonald et al., 2011). Fast-growing population in cities is accompanied by rapid urban expansion, the potential effect of which is to drive significant local and regional climate change (Argüeso et al., 2014; Chen & Frauenfeld, 2016; Chow et al., 2012; Georgescu et al., 2013; Grimm et al., 2008; Zhou et al., 2004). A typical example of urbanization's impacts on local climate is the urban heat island (UHI) effect (Kalnay & Cai, 2003; Thompson & Perry, 1997). Compared to natural land surface, urban surface is commonly characterized by high heat-storage capacity, tall buildings, large impervious zone, and less vegetation. Continued conversion of natural surface to urban landscape will inevitably affect surface energy balance and the structure of the boundary

layer (Benson-Lira et al., 2016; Georgescu et al., 2009a). Although UHI generally has negligible effects on global climate, its influence on local urban climate can be comparable to changes induced by global greenhouse gas emissions (Grimm et al., 2008; Kong et al., 2020; Krayenhoff et al., 2018; Liao et al., 2018; Yang et al., 2017). Therefore, it is of great significance to understand how much urbanization modifies the local climate in fast-growing cities (Cao et al., 2016; Georgescu, 2015; Georgescu et al., 2013).

UHI effect was first observed in London (Howard, 1833), and it was further explored at other places in the world by a number of studies. For example, Kalnay and Cai (2003) reported that the surface temperature increase induced by land use changes and urbanization was 0.27°C per century in the United States. Phoenix Metropolitan Area in the southwestern U.S. experienced extensive land cover alteration since 1950 (Chow et al., 2012). Consequently, mean regional temperature of this region in 2001 was 0.12°C warmer than that in 1973. In areas where greater urbanization occurred, the temperature difference could even exceed 1°C (Georgescu et al., 2009a, 2009b).

China, as one of the largest developing countries, experienced unprecedented economic development and urban expansion since the 1980s. Based on meteorological observations and National Centers for Environmental Prediction (NCEP) reanalysis products, Zhou et al. (2004) determined that urban expansion in the southeast of China during 1970–1998 resulted in 0.05°C/decade temperature increase. In the northern China, the warming magnitude of surface air temperature caused by urbanization from 1961 to 2000 was 0.11°C/decade (Ren et al., 2008). Du et al. (2007) estimated that the mean annual air temperature increased 0.28°C–0.44°C/decade over 1991–2005 in urban areas of the Yangtze River Delta (YRD), much larger than that in the surrounding rural areas (0.04°C–0.20°C/decade).

In previous studies, the UHI effect was generally investigated by comparing temperature at urban stations to the rural ones (Du et al., 2007; Hua et al., 2008; Ren et al., 2008). This urban minus rural (UMR) method is highly dependent on how urban/rural stations are classified (Kalnay & Cai, 2003; Zhou et al., 2004) and there can be large uncertainties. Population or nighttime light data were typically used to classify urban and rural stations. Several factors might yield bias in the UMR-derived results, especially in China. First, most meteorological stations are located inside or near the cities and very few stations can be precisely categorized as rural stations, which impacts the accuracy of rural temperature estimation. Second, a rural station can become an urban one, for the continuous expansion during urbanization makes the classification of stations dynamic. In most UMR-based studies, the types of stations were unchanged throughout the entire study period, which underestimated the UHI effect if the conversion from rural to urban was ignored (Yang et al., 2011). Yang et al. (2011) developed a dynamic classification scheme using nighttime light records and found that rapid urbanization had more evident influence on surface warming in East China. In recent years, researchers applied this dynamic classification into studies about urbanization effects on warming temperature, extreme heat waves, heat stress, and atmospheric moisture (Kong et al., 2020; Liao et al., 2018; Lin et al., 2018; Luo & Lau, 2019; Yang et al., 2017). Nonetheless, this approach is challenged by the fact that rural stations near cities may be influenced by horizontal urban heat advection process (Cosgrove & Berkelhammer, 2018; Heaviside et al., 2015). The estimated warming trend based on the dynamic UMR method might still be underestimated (Yang et al., 2011).

Numerical models have been commonly employed to quantify the impact of urbanization on regional climate in China. Some studies focus on single city, such as Beijing (Miao et al., 2009; Yang et al., 2016), Nanjing (Yang et al., 2012), Hangzhou (Chen et al., 2014), and Wuhan (Ke et al., 2013). Three Chinese largest megalopolis, Beijing-Tianjin-Hebei (BTH), Pearl River Delta (PRD), and Yangtze River Delta (YRD) have also been explored as the study domain in earlier publications (Cao et al., 2016; Liao et al., 2014; Lin et al., 2016; Wang et al., 2012, 2013, 2014; Zhang et al., 2010). However, evaluation based on numerical simulation can be improved. The urban effects reported in many of these studies were not supported with historic observations. Also, these modeling studies typically designed simulations by utilizing two most extreme scenarios of land use and land cover (LULC), preurban and posturban, into climate modeling over the last 4 decades in China. The dynamic feature of the entire period was not fully captured by two extreme endpoints. Generally, urbanization in China can be divided into three different stages, slow urbanization prior to 1980s, medium-speed urbanization in 1990–2000, and rapid urbanization after 2000 (Xiao et al., 2014). The UHI effect may change through different stages and the corresponding temporal variations usually remain underexplored.

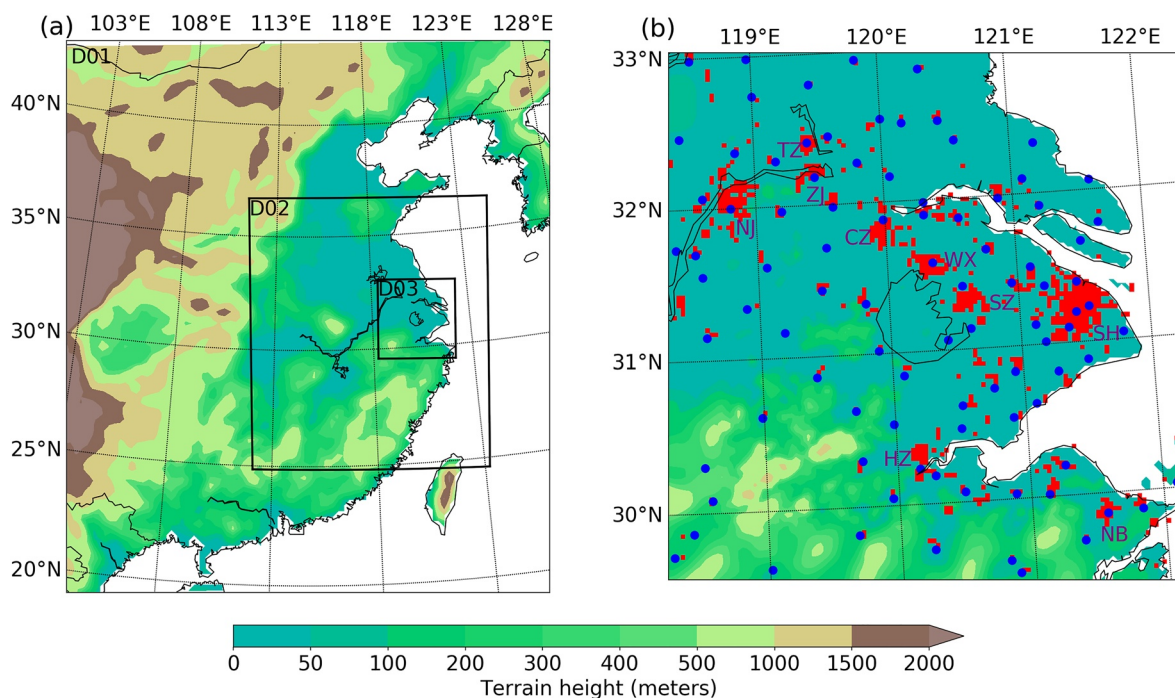


Figure 1. Weather Research and Forecast (WRF) domain configuration and meteorological stations. (a) Three one-way nested domains for WRF simulations. (b) Domain 03 (D03) and observational meteorological stations (blue dots). The urban extent of 2010 in Yangtze River Delta (YRD) is shown in red with initials of the cities. NJ, TZ, ZJ, CZ, WX, SZ, SH, HZ, and NB represent cities of Nanjing, Taizhou, Zhenjiang, Changzhou, Wuxi, Suzhou, Shanghai, Hangzhou, and Ningbo, respectively.

The Yangtze River Delta (YRD) metropolitan region experienced significant urbanization over the last 30 years and became one of the most developed areas in China. Previous works on YRD investigated the UHI effect based solely on either static classification scheme (Du et al., 2007) or numerical modeling (Cao et al., 2016; Chen & Zhang, 2018; Wang et al., 2012) without analyzing observational records. In this study, we combined both the historic observations and numerical modeling to quantitatively evaluate the impacts of urban expansion on YRD's surface air temperature. By incorporating multiple land cover scenarios into mesoscale climate simulation, we assessed the urban climatic effects during different historical periods in YRD and further explored the mechanism.

2. Data and Methods

2.1. Meteorological Observations

There are 93 meteorological stations operated by the China Meteorological Administration publicly available in our study domain (D03, as shown in Figure 1b). Daily records of average 2-m air temperature (T_{mean}), minimum temperature (T_{min}), and maximum temperature (T_{max}) at these stations were obtained from China Meteorological Data website (<http://data.cma.cn/en>). We excluded the stations with five or more missing records in any summer, and the remaining 85 stations were utilized in analyzing the trend over 1980–2018.

Based on geographical location and the surrounding environment, we dynamically classified the 85 stations in D03 into urban and rural categories. Similar to Liao et al. (2018) and Kong et al. (2020), we classified these stations according to dynamic land-use and land-cover data (LULCD) as described in Section 2.3. The LULCD is available in 1990, 1995, 2000, 2005, 2010, and 2015, and our study period was divided into six subperiods (Table 1). Each subperiod shared the built-up area using the LULCD map at the beginning year of the subperiod, except that the first one (1980–1994) used LULCD of 1990. We established buffer zones (area within 4 km of each station) and then calculated the urban area ratio within the buffers based on the built-up area in each subperiod. Stations with urban ratio greater than 33% were classified into urban type and the others were classified as rural ones. There were 14 urban stations in 1990, and the number became 46 in

Table 1
Division of Study Period, LULCD, and Number of Urban Stations That Each Subperiod Corresponds to

Subperiods	1980–1994	1995–1999	2000–2004	2005–2009	2010–2014	2015–2018
LULCD	1990	1995	2000	2005	2010	2015
Number of urban stations	14	18	22	34	38	46

the year 2015 (Table 1). We compared the trends of 2-m air temperature at urban stations with the rural ones to assess the impact of urbanization. Linear regression was employed to estimate the trends in temperature and Student's *t*-test was applied to determine the statistical significance. These station observations were also employed to evaluate the performance of the configured climate model during 2000–2004 (Section 2.5). We utilized LULCD of 2000 to classify these 93 stations, and there were 26 urban stations and 67 rural ones.

2.2. Model Configuration

To reproduce the climate in YRD and assess the impacts of urbanization, we used the Weather Research and Forecasting (WRF-ARW, version 3.7.1) model (Skamarock et al., 2008) to perform numerical experiments. The WRF model was centered at 31.5°N/114.7°E and configured with three one-way nested domains (Figure 1). The domains had horizontal grid spacing of 27, 9, and 3 km, respectively. The horizontal grids of the outer domain (D01) were 99 × 89, which covered most mainland of China and extended to the oceans. YRD was influenced by East Asian monsoon, and D01 provided the large-scale circulation background for intermediate and innermost domains (D02 and D03). D02 covered most part of East China and part of Yellow Sea and East China Sea (147 × 129 horizontal grids). The innermost domain (D03), covering the whole YRD, was the key region where sensitivity simulations were performed and analyzed in detail. The size of D03's horizontal grid was 129 × 126. There were totally 30 levels in the vertical direction, and the upper boundary was set at 50 hPa. The time steps for three domains were 180, 30, and 15 s; output intervals for three domain simulation were 6, 3, and 3 hr, respectively. The initial boundary conditions were provided by the National Centers for Environmental Prediction (NCEP) Global Final Analysis (FNL, <https://rda.ucar.edu/datasets/ds083.2/>) with a horizontal resolution of 1° × 1° and a time interval of 6 hr. The "sst_update" option was turned on for the three domains to update the low boundary conditions every 6 hr. The simulations were implemented for the five summers (June, July, and August) over 2000–2004. The WRF model was run from May 23 to August 31 in each summer (the first 9 days were performed as model spin-up).

The main parameterization of our WRF simulations is reported in Table 2. We applied the Kain-Fritsch cumulus scheme in D01 and D02 but not in the high-resolution simulation of D03. The Single-Layer Urban Canopy Model (SLUCM; Kusaka & Kimura, 2004) was coupled with Noah land surface model (Chen et al., 1996) to simulate urban thermodynamic and land-atmosphere interactions. In WRF-SLUCM, urban land cover category is divided into three subtypes: low-intensity residential, high-intensity residential, and industrial/commercial. In our simulations, we used high-intensity residential to represent urban cover in YRD as previous studies did in similar regions (Cao et al., 2016, 2018; Wang et al., 2012, 2015). All the urban pixels were set to have 90% impervious surface (building roof, wall, and road) and 10% urban vegetation as in Cao et al. (2016). Urban vegetation was prescribed as cropland/grassland mosaic category in the WRF-SLUCM model, for the cropland/grassland mosaic was similar to the urban vegetation in YRD. The main urban parameters are provided in Table S2 in Supporting Information S1.

2.3. Land-Use and Land-Cover Data (LULCD)

The land-use data from the National Land Use Change Database (Liu et al., 2014) is derived from Landsat TM images by the Chinese Academy of Sciences (CAS). The spatial resolution of this product is 1 km. The data set contains six major land cover classes (agriculture, forest, grassland, water, urban, and not-use area) and 26 minor classes (details of land use classification of CAS LULCD can be found at <http://www.dsac.cn/DataProduct/Detail/200804>). The unused land is mainly covered by barren rock, the area of which is <0.1% of YRD's total area. Therefore, only the other five major land cover types (agriculture, grassland,

Table 2
Main Schemes in WRF

	D01	D02	D03
WRF Version			3.7.1
Horizontal grid spacing	27 km	9 km	3 km
Grid numbers	99 × 89	147 × 129	129 × 126
Vertical levels		30	
Time steps	180 s	30 s	15 s
Longwave radiation scheme		Rapid Radiative Transfer Model (RRTM)	
Shortwave radiation scheme		New version of RRTM (RRTMG)	
Cumulus scheme		Kain-Fritsch	Null
Microphysics scheme		WRF Single-Moment 3-class (WSM3)	
Planetary boundary layer (PBL) scheme		Yonsei University (YSU) PBL scheme	
Surface layer scheme		Eta similarity	
Land surface model		NOAH	
Urban module scheme		Single-Layer Urban Canopy Model (SLUCM)	

water, forest, and urban) were included in the analyses of urban expansion in YRD. We selected LULCD of 1990, 1995, 2000, 2005, 2010, and 2015 to explore urban cover changes over the years (red zone in Figure 2).

The default LULCD in the WRF model is the United States Geological Survey (USGS) 24-category land-use data produced in 1993. Since the land cover in YRD changed dramatically over these years due to fast urbanization, the static USGS data cannot well represent these characteristics of the region. The LULCD used in our simulations was updated according to CAS LULCD. Land cover classification in CAS data set is different

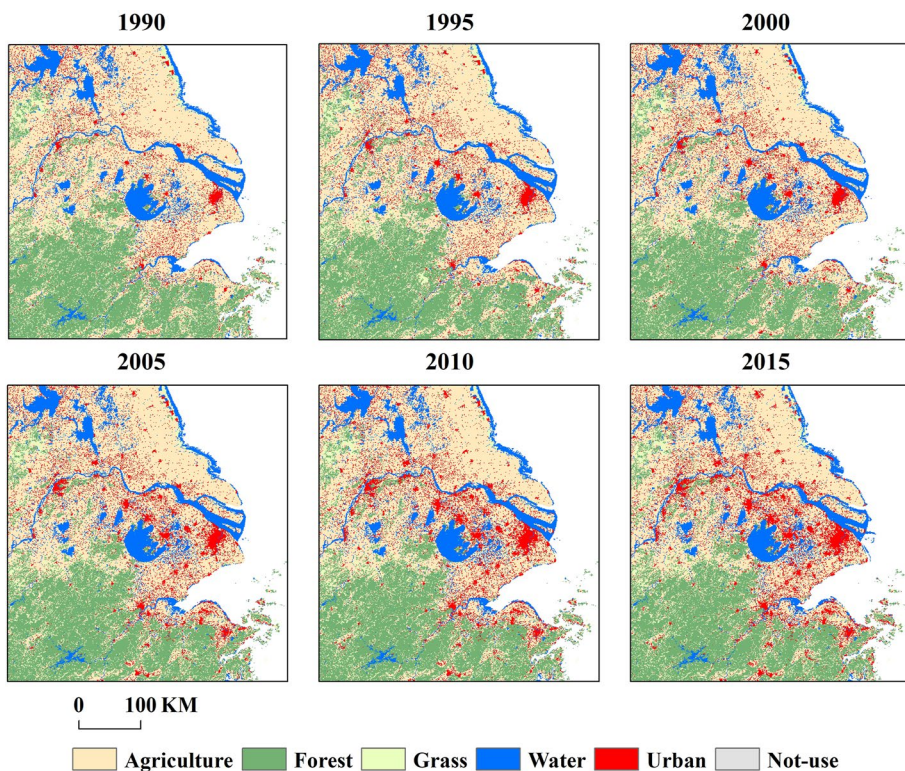


Figure 2. Land use and land cover from 1990 to 2015 in Yangtze River Delta (YRD).

Table 3
Design of the WRF Simulations

Simulations	LULCD	Simulation time	
		Spin-up time	Time for analysis
S2000 (control run)	2000	23–31/05/2000–2004	01/06–31/08/2000–2004
S1990	1990	23–31/05/2000–2004	01/06–31/08/2000–2004
S2010	2010	23–31/05/2000–2004	01/06–31/08/2000–2004

from USGS, and we manually reclassified the CAS categories into USGS 24 categories (detailed conversion is provided in Table S1 in Supporting Information S1). After the conversion, we resampled the CAS data set to 3-km grid based on majority resampling principle in ArcGIS. The projected coordinate of CAS data set was Krasovsky_1940_Albers, and Lambert conformal conic projection was employed in domain's horizontal coordinates. The resampled 3 km data sets were then mapped to the grid of D03 based on the nearest neighbor principle. We selected LULCD of 1990, 2000, and 2010 to represent land surface at different stages of urbanization. The LULCD of CAS was only used in the innermost domains (D03), and the WRF's default LULCD was kept for the two outer domains as in Cao et al. (2016).

2.4. Experimental Design

We performed three numerical experiments (S1990, S2000, and S2010) using LULCD of 1990, 2000, and 2010 to capture urbanization-induced warming (Table 3). We first implemented a control run with LULCD of 2000 from 2000 to 2004 to evaluate the performance of the atmospheric model. We also designed two other sensitivity runs (S1990 and S2010 in Table 3) by incorporating historical land cover scenarios into the model. All the configurations in sensitivity runs were identical to S2000 except that the land cover was replaced by LULCD of 1990 and 2010 (Table 3).

2.5. Model Evaluation

We used observed temperature data at 93 meteorological stations to evaluate the WRF model performance. The station data includes daily T_{mean} , T_{min} , and T_{max} records. For each station, we selected three statistical metrics, bias (BIAS), root mean square error (RMSE), and correlation coefficient (CC), to evaluate the accuracy of temperature in numerical modeling. The evaluation metrics were calculated as

$$\text{BIAS}_j = \frac{\sum (\text{Sim}_{ij} - \text{Obs}_{ij})}{T} \quad (1)$$

$$\text{RMSE}_j = \sqrt{\frac{\sum (\text{Sim}_{ij} - \text{Obs}_{ij})^2}{T}} \quad (2)$$

$$\text{CC}_j = \frac{\sum (\text{Sim}_{ij} - \overline{\text{Sim}}_j)(\text{Obs}_{ij} - \overline{\text{Obs}}_j)}{\sqrt{\sum (\text{Sim}_{ij} - \overline{\text{Sim}}_j)^2 \sum (\text{Obs}_{ij} - \overline{\text{Obs}}_j)^2}} \quad (3)$$

where j is the index of the station, i is the index of time, Obs_{ij} is daily observed records for station j , and Sim_{ij} is simulated time series at the grid cell closest to station j . T is the total length of the simulation period (460 days).

2.6. Climatic Effects of Historical Urbanization

We compared daily mean (T_{mean}), minimum (T_{min}), maximum (T_{max}) air temperature, and diurnal temperature range (DTR) at 2-m height extracted from different numerical experiments (S1990, S2000, and S2010). The difference between S2000 and S1990 simulations was denoted as S2000–S1990, so were the S2010–

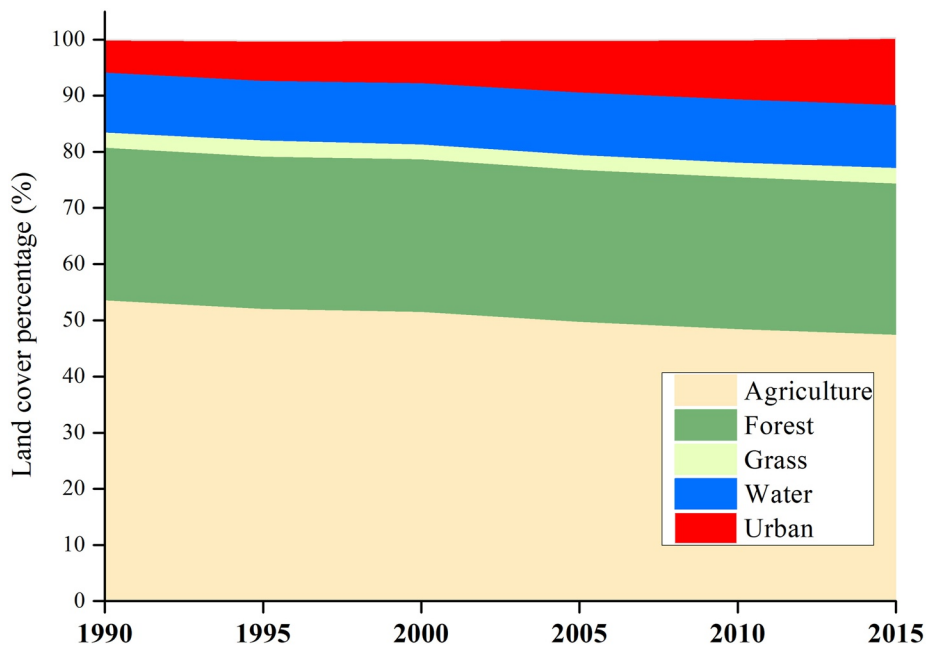


Figure 3. Changes in different land use and cover from 1990 to 2015 over the Yangtze River Delta (YRD).

S2000 and S2010–S1990. S2010–S1990 represented the overall impacts of long-term urbanization over the 20 years, and S2000–S1990 and S2010–S2000 characterized the signals of urban expansion in the early stage (1990–2000) and the late stage (2000–2010).

We employed effect index (EI) to assess spatial influence of urban expansion-induced warming (Cao et al., 2016; Zhang et al., 2010). The EI was calculated as

$$EI = \frac{A_{\text{change}}}{A_{\text{urban}}} \quad (4)$$

where A_{change} denotes the areas where the urbanization-induced increase in near-surface temperatures (T_{mean} , T_{min} , and T_{max}) exceeded 0.1°C , and A_{urban} denotes total urban areas after corresponding urban expansion. When $EI = 1$, it means that only urban pixels are affected; <1 , indicates that part of urban pixels are affected; >1 , urban effects extend beyond urban pixels to surrounding areas.

3. Results

3.1. Urban Land Development and Impacts on Observed Air Temperatures

Area of forest, grass, and water did not change much while urban area doubled during 1990–2015 (Figure 3). Percentage of urban area in D03 increased from 5.99% in 1990, to 7.28% in 1995, 7.77% in 2000, 9.51% in 2005, 10.81% in 2010, and 12.08% in 2015. We also found in Figure 3 and Figure S1 in Supporting Information S1 that urban expansion in YRD primarily reduced agricultural areas, which is consistent with the results in Hao et al. (2018). Changes of urban area per 10 years (Figure S1 in Supporting Information S1) demonstrated that the urbanization process can be divided into two stages, medium-speed growth in early stage of urbanization (1990–2000) and high-speed growth in late stage (after 2000).

Both the urban and rural stations were showing significant warming trends in T_{mean} , T_{min} , and T_{max} (Figure 4). However, urban stations experienced a greater warming magnitude than rural: 0.51 versus $0.39^{\circ}\text{C}/\text{decade}$ for T_{mean} , 0.49 versus $0.40^{\circ}\text{C}/\text{decade}$ for T_{min} , and 0.60 versus $0.45^{\circ}\text{C}/\text{decade}$ for T_{max} . Urbanization imposed a greater warming effect on urban climate in YRD. T_{min} had largest urban-rural contrast, and the difference in T_{max} was the smallest but still positive. The average urban-rural differences in T_{mean} were 0.05, 0.17, 0.42, and 0.38°C during 1980, 1990, 2000, and 2010–2018, respectively. Urban-rural 2 m temperature

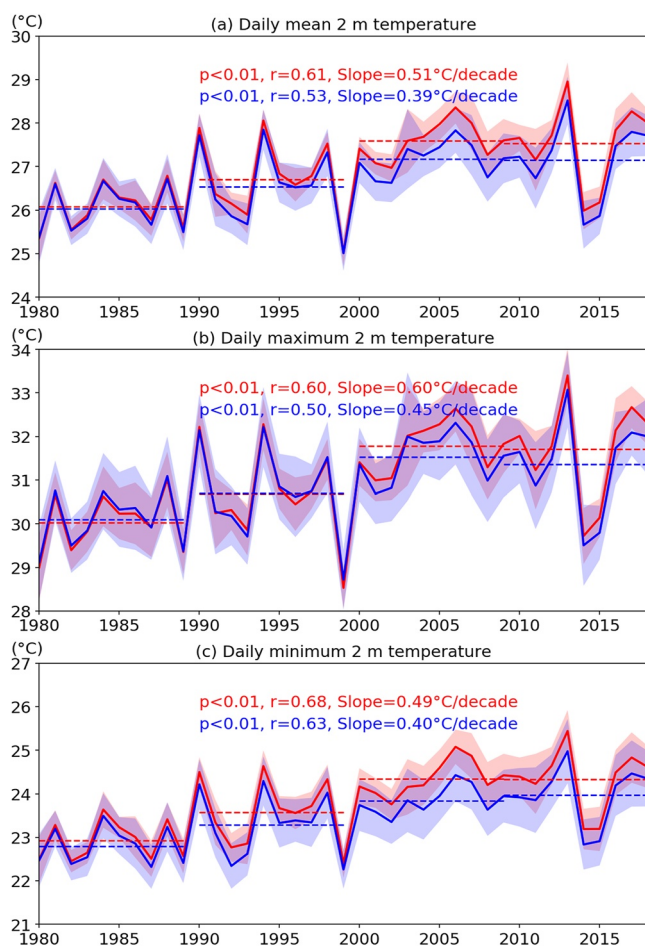


Figure 4. Annual time series plots of summertime (a) T_{mean} , (b) T_{max} , and (c) T_{min} averaged over urban (red) and rural stations (blue) during 1980–2018. The shaded areas represent one standard deviation above and below the mean. Dash lines show decadal averages during 1980–1989, 1990–1999, 2000–2009, and 2010–2018. Statistics of the linear regressions for 1980–2018 are reported.

difference was much larger after 2000 than before (especially for T_{mean} and T_{min}), which demonstrated that the late stage of urbanization exerted stronger warming impacts.

3.2. Model Evaluation

Table 4 presents evaluation metrics derived from model simulation and station records. The BIAS, RMSE, and CC between observed and simulated T_{mean} were 0.90, 2.0, and 0.83, respectively. The WRF model performed slightly better in rural stations than in urban stations. The correlation coefficients were generally high, especially at the urban stations (Figure 5a). Our simulated T_{mean} matched better with the observations than several other WRF-based studies on urban agglomeration in China (Cao et al., 2016; Miao et al., 2009; Wang et al., 2012, 2015; Yang et al., 2014). WRF simulated T_{min} were also in good agreement with the observations (BIAS 0.12, RMSE 1.95, and CC 0.82) while T_{max} exhibited the largest differences between the simulation and observations (BIAS 1.14, RMSE 2.77, and CC 0.79). Most stations had slightly lower CC of T_{max} compared to T_{mean} and T_{min} (Figure 5); however, the evaluation metrics of T_{max} were still satisfactory. Moreover, the simulated daily temperature was able to capture the temporal variability of the observational values in both urban and rural stations (Figure 6, Figures S2 and S3 in Supporting Information S1).

Overall, both the temporal and spatial patterns of the near-surface temperature extracted from the WRF experiments were close to the patterns from observational records, indicating that our simulation was viable and suitable for further evaluating the effects of urban expansion.

3.3. Impacts of Historical Urbanization on Near-Surface Air Temperature

Simulated results showed that increases in T_{mean} , T_{min} , and T_{max} induced by urban expansion during 1990–2010 were significant (Figure 7). The warming effects were greater in urban regions than rural, and the pixels with large temperature increase ($>1^\circ\text{C}$) were the surroundings of urban center (i.e., newly built urban areas). The influence of urban warming

Table 4

Comparison of the Simulated Average Daily Mean Temperature (T_{mean}), Daily Maximum Temperature (T_{max}), and Daily Minimum Temperature (T_{min}) With Observational Values, Along With the Mean Bias (BIAS), Root Mean Square Error (RMSE), and Correlation Coefficient (CC) of T_{mean} , T_{max} and T_{min} for All the Stations (All), Urban Stations (Urban) and Rural Stations (Rural)

	T_{mean}			T_{max}			T_{min}		
	All	Urban	Rural	All	Urban	Rural	All	Urban	Rural
OBS ^a	27.08	27.31	27.00	31.35	31.45	31.31	23.87	24.05	23.63
WRF ^b	27.99	28.39	27.83	32.49	32.89	32.33	23.75	24.22	23.74
BIAS ^c	0.90(± 0.63)	1.08(± 0.59)	0.84(± 0.63)	1.14(± 1.02)	1.43(± 0.81)	1.02(± 1.07)	0.12(± 0.67)	0.17(± 0.62)	0.01(± 0.68)
RMSE ^c	2.00(± 0.34)	2.06(± 0.37)	1.98(± 0.33)	2.77(± 0.35)	2.79(± 0.40)	2.77(± 0.32)	1.95(± 0.19)	1.94(± 0.17)	1.95(± 0.20)
CC ^c	0.83(± 0.02)	0.84(± 0.02)	0.83(± 0.03)	0.79(± 0.02)	0.79(± 0.02)	0.78(± 0.02)	0.82(± 0.02)	0.82(± 0.02)	0.83(± 0.03)

^aThe statistics were averaged across stations of all, urban, and rural. ^bThe statistics were averaged across the grid cells which were nearest to the stations of all, urban, and rural. ^cThe statistics were averaged values over the stations and corresponding nearest grid cells, and the values in parentheses represent the standard deviations.

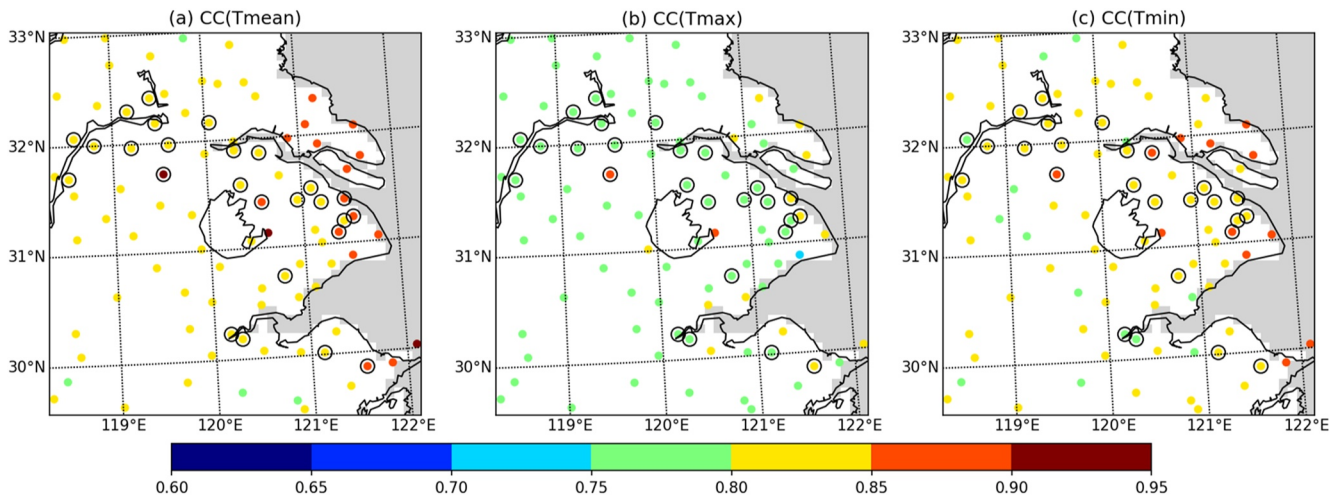


Figure 5. Correlation coefficients of the Weather Research and Forecast (WRF) simulated and observed (a) T_{mean} , (b) T_{max} , and (c) T_{min} in five summers (2000–2004) at the 85 stations. Urban stations are marked with black circles.

effect was not confined to urban areas. Regionally, simulations of S2010–S1990 showed that urban expansion during this period increased YRD's T_{mean} by 0.13°C .

Based on the WRF simulation, the 20-year urban expansion increased the summertime T_{mean} , T_{min} , and T_{max} in urban areas by 0.75 , 1.06 , and 0.45°C (averaged across all urban pixels in 2010), respectively (Figure 8). The increasing trend in temperature was consistent with the urban-rural trend contrast in Figure 4. Generally, urbanization had a greater effect on T_{min} than T_{max} , which matched with urban-rural temperature difference in Section 3.1. Increases in T_{min} of S2010–S1990 lasted through the whole summer, but the warming effect on T_{max} mainly appeared in July and August, with least in June (Figures 9 and 10). Additionally, the warming magnitude of T_{min} had relatively small spatial standard deviations throughout the summertime (Figure 9). Therefore, these results demonstrated that an overwhelming majority of urban pixels exhibited increased T_{min} across the whole summer. On the other hand, responses of T_{max} to urbanization had greater uncertainties, for some urban pixels might show decreases in T_{max} . Nevertheless, the average of T_{max} over the urban areas reflected an obvious warming effect across the summer ($+0.45^{\circ}\text{C}$). The magnitude of increase in T_{mean} ($+0.75^{\circ}\text{C}$) over S2010–S1990 was between that of T_{min} and T_{max} , and the warming magnitude of summertime T_{mean} was strongest in July. These results indicated that urbanization-induced warming effect was mainly reflected on nighttime air temperature, especially during 20:00–08:00 (Figure 10), with least warming magnitude during daytime. Different warming magnitudes between T_{min} and T_{max} resulted in reduced DTR in the cities and the surrounding areas. The decrease in DTR exceeded 0.1°C in most part of the YRD, and the pixels with the greatest reduction in DTR were also located in the newly built urban areas ($<-0.6^{\circ}\text{C}$ as shown in Figure 7).

It is worth noting that the urban warming effects varied across different stages of urbanization. In the early stage (1990–2000), the warming effect on T_{mean} was quite limited and mainly confined to the newly built regions (Figure 7). The warming effect in S2010–S2000 extended to a larger area. T_{mean} increases were observed around the Lower Taihu watershed, where quite a few cities including Changzhou, Wuxi, Suzhou, and Shanghai are located. The expansion of the area affected by warming was also confirmed by higher EI values. EI of T_{mean} was 3.49 in 2000, and that number increased to 5.66 in 2010 (Table 5), indicating the warming effect was enhanced in the late stage. The urban area varied in different stages of urbanization, and we examined the average warming magnitude over urban area at each stage. Changes in T_{mean} of S2000–S1990 and S2010–S2000 were calculated and averaged across the urban pixels for 2000 and 2010, respectively. The warming magnitudes of T_{mean} over S2000–S1990 and S2010–S2000 were 0.49 and 0.51°C , respectively (Figure 8). This enhanced warming effect over urban area existed through the entire summer and became especially significant in July (Figure 9).

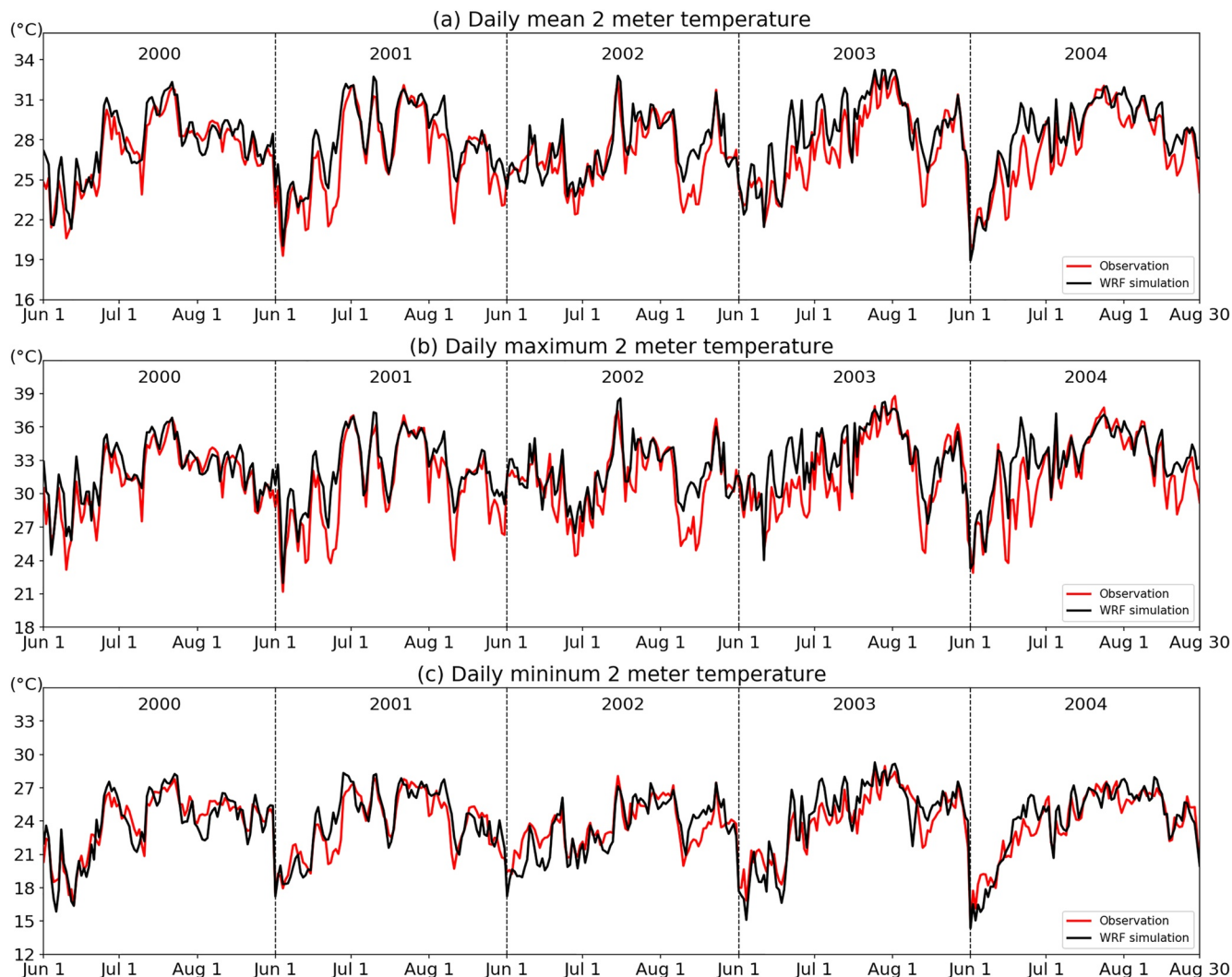


Figure 6. Simulated (black) and observed (red) time series of (a) T_{mean} , (b) T_{max} , and (c) T_{min} averaged across all the stations in the five summers (2000–2004).

The enhanced warming effect on T_{min} was more substantial than that on T_{mean} (Figures 7–9). Regional warming effects were discernible at early urbanization (1990–2000) and reinforced after another 10 years of urbanization (2000–2010). EI of T_{min} was 3.27 in 2000, and it rose to 5.75 in 2010 (Table 5). Urban sprawl from 1990 to 2000 increased T_{min} at urban pixels by 0.68°C and the effect was even stronger during 2000–2010 ($\Delta T_{\text{min}} = +0.76^{\circ}\text{C}$). Warming magnitudes of T_{min} in both urbanization stages were greater than T_{mean} (Figure 8). Compared to T_{mean} and T_{min} , the warming magnitude of T_{max} was smaller. T_{max} increased 0.31 and 0.28°C for S2000–S1990 and S2010–S2000 (Figure 8), respectively. The decline in DTR also became larger in the second stage (-0.37°C of S2000–S1990 versus -0.48°C of S2010–S2000) as shown in Figure 8.

3.4. Potential Influence on Heat Stress

Near-surface air temperature and humidity typically play a key role in the heat risk issue. We found that average 2-m water vapor mixing ratio (Q2) over the urban areas decreased during the 1990–2010 urban expansion with a reduction of 0.56 g/kg (Figure 11). The decrease in Q2 was limited and mainly concentrated on newly built areas in the early stage (Figure 11a), while urban dry island (UDI) effect extended to a larger region beyond city boundaries in the late stage of urbanization. The urban low-level air moisture loss was greater in the daytime than that in the nighttime (Figure 11e), and it reached the peak at 14:00 local time ($>1 \text{ g/kg}$ for S2010–S1990). The UDI effect intensified with urban sprawl in YRD (Figure 11e). Previous

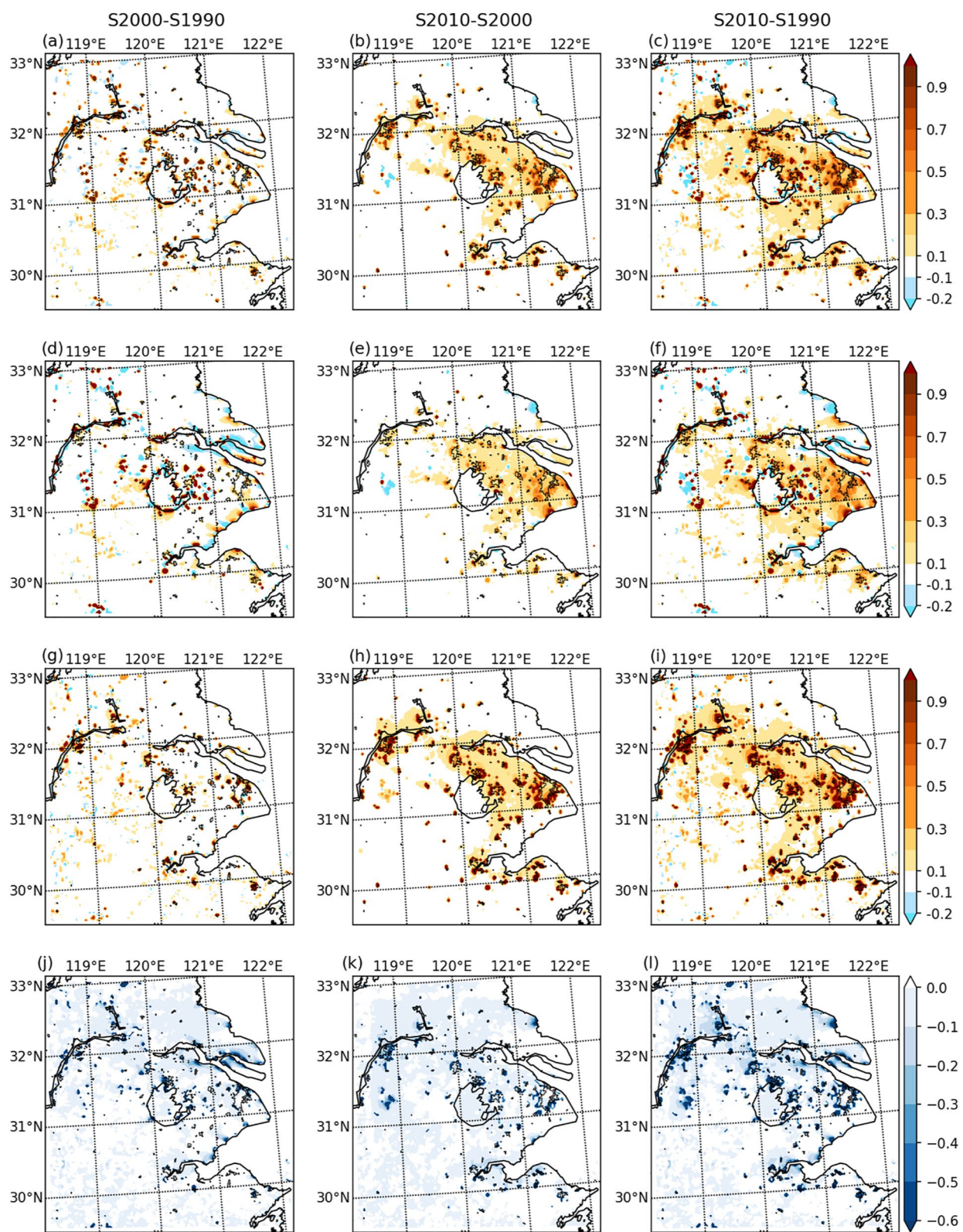


Figure 7. Spatial changes of summertime T_{mean} (a–c), T_{max} (d–f), T_{min} (g–i), and diurnal temperature range (DTR; j–l) Derived from Weather Research and Forecast (WRF) simulation comparison: S2000–S1990 (left column), S2010–S2000 (middle column), and S2010–S1990 (right column).

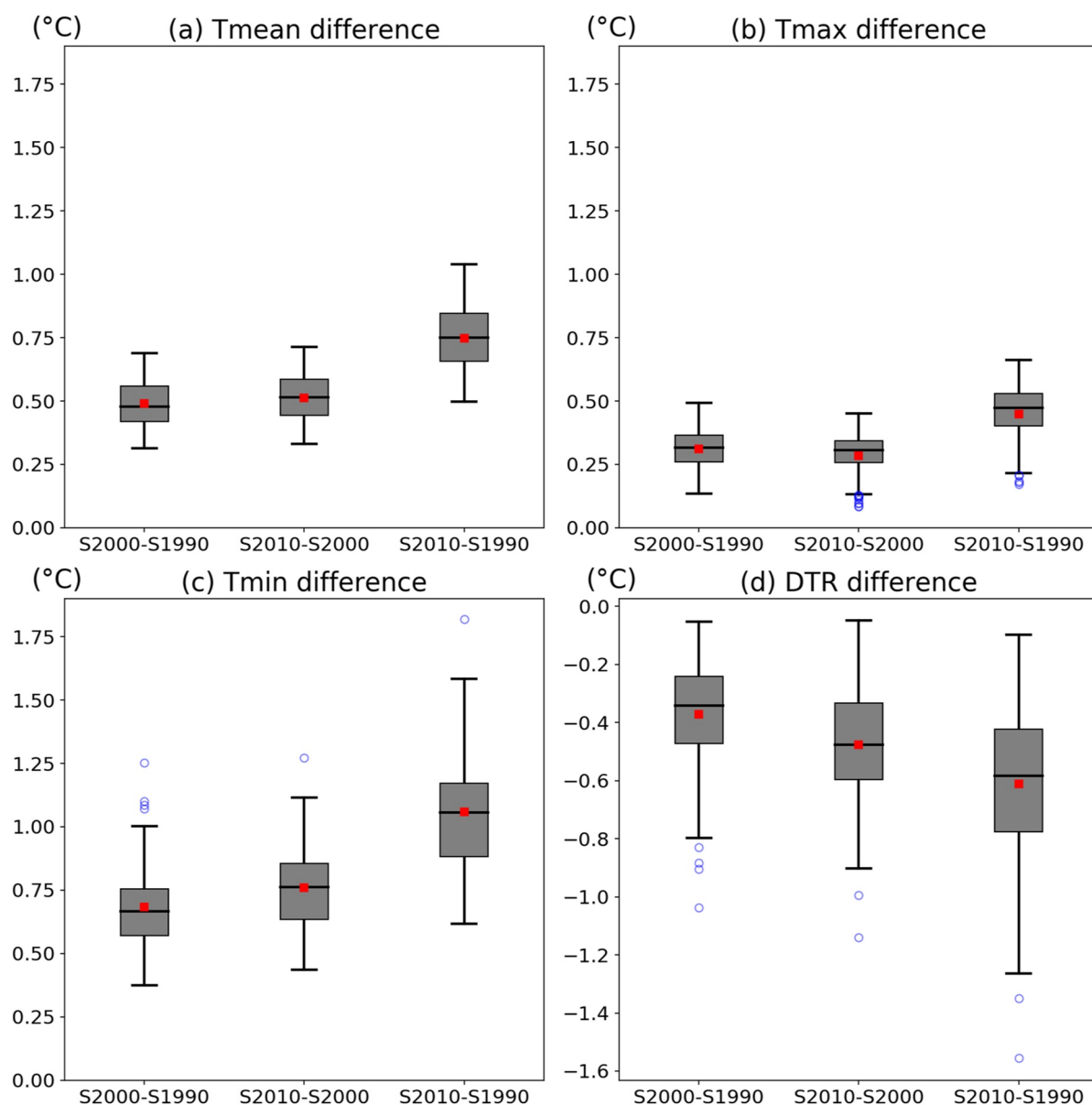


Figure 8. Boxplot of changes in (a) T_{mean} , (b) T_{max} , (c) T_{min} , and (d) Diurnal temperature range (DTR) during the summers (S2000–S1990, left bar in every panel; S2010–S2000, middle bar; S2010–S1990, right bar). These boxplots are generated by incorporating results at all the urban pixels.

studies focused on the YRD also found that urbanization dried out the atmosphere and the UDI effect was closely related to the loss of vegetated cover during urbanization (Hao et al., 2018; Luo & Lau, 2019).

The UDI effect can counteract the influence of warming temperature on urban heat stress. In this study, a simplified wet-bulb globe temperature (WBGT) was employed to assess heat stress. The WBGT is defined as $\text{WBGT} = 0.567 T + 0.393e + 3.94$, where T is 2-m air temperature in Celsius and e is the actual vapor pressure in hPa (Willett & Sherwood, 2012). WBGT Values <26 indicate low heat risk; values between 26 and 28 mean moderate heat risk; values between 28 and 32 represent high heat risk; values greater than 32 mean extreme high heat risk to human health.

We found that urbanization-induced changes in heat stress were rather small over urban areas (Figure 12), which was due to the fact that the UDI effect offset the heat stress. The average increase over urban area was 0.04, 0.05, and 0.07 for S2000–S1990, S2010–S2000, and S2010–S1990, respectively (Figure 12d). Figure 12e demonstrated that heat stress increase tended to be higher in June. Figure 12f presents the diurnal cycle of

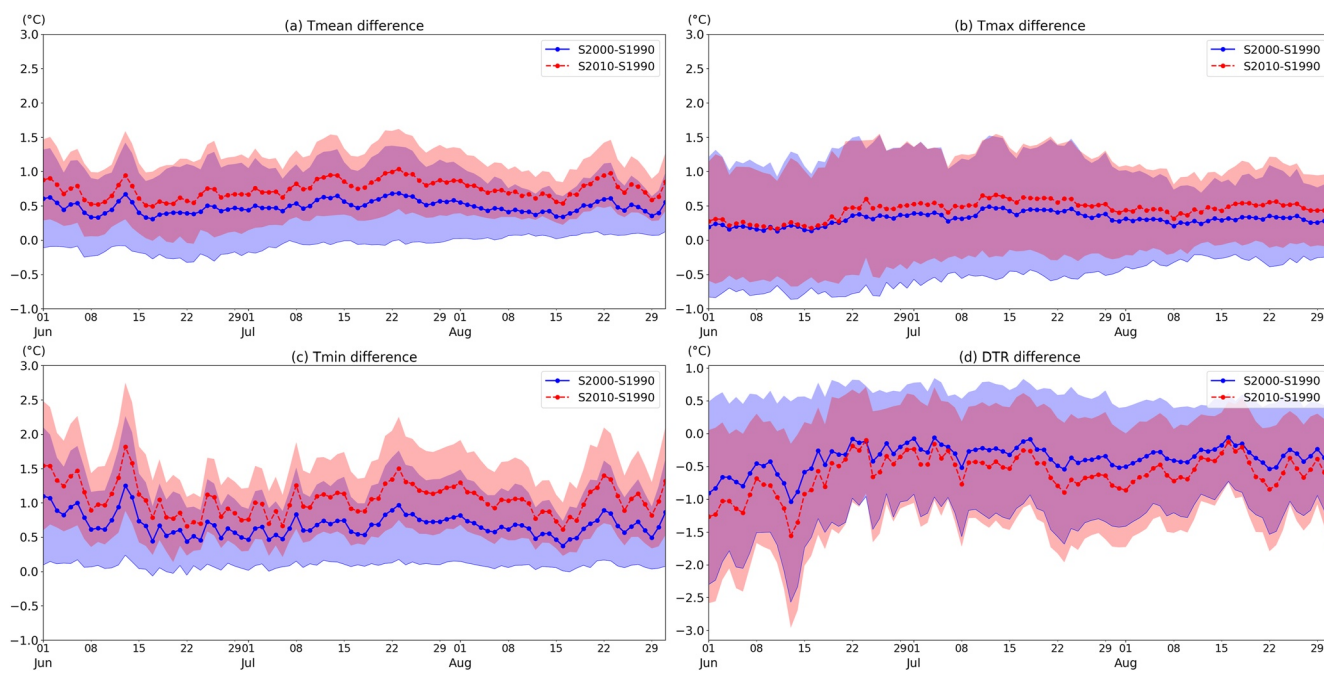


Figure 9. Time series of changes in (a) T_{mean} , (b) T_{max} , (c) T_{min} , and (d) Diurnal temperature range (DTR) derived from S2000–S1990 (blue) and S2010–S1990 (red). The result of S2000–S1990 was the average across all urban pixels of 2000, and the S2010–S1990 results were averaged over all urban pixels of 2010. Shaded areas indicate one spatial standard deviation above and below the average.

summertime heat stress extracted from different simulations, which revealed that in the night (20:00–08:00 at local time) urbanization obviously raised the heat stress index (up to 0.5 units). However, urbanization reduced WBGT during the daytime, which might be related to significant moisture loss in the low-level atmosphere (Figure 11e). It should be noted that although the changes of heat stress index values were small, urban-induced increase in heat stress was enhanced in the late stage of urbanization.

3.5. Energy Balance and Partitioning

The differences between these simulations originated from the modification of LULCD, which substantially affected energy-related processes and land-atmosphere interactions near the surface. In our WRF simulations, surface sensible heat and latent heat fluxes were simulated by the Noah land surface model (LSM) and then passed to planetary boundary (PBL). To explore possible causes for this warming effect, energy balance, and energy partitioning were further investigated.

The land surface energy fluxes directly influence the air temperature, and they are highly dependent on net solar radiation absorbed by the surface. Modification of LULCD altered land surface albedo, which subsequently affected the net shortwave radiation. We compared the surface energy balance in S2010 and S1990 experiments. The albedo decreased slightly in newly built urban region ($\Delta \text{Albedo} = -0.08$; Figures S4 and S5 in Supporting Information S1). Therefore, net shortwave radiation increased in the urban areas, resulting on average a 5.71 W/m^2 increase over 1990–2010 (Figure S5 in Supporting Information S1). However, net radiation dropped 25.46 W/m^2 in the urban pixels (Figure S5 in Supporting Information S1), for net longwave radiation suffered a great loss due to urban expansion, especially in the daytime (Figures S4–S6 in Supporting Information S1). Higher surface temperature during the daytime in the urban area led to stronger upward longwave radiation (Figures 13 and 14) and therefore lowered the net radiation.

There were significant differences between the responses of sensible heat and latent heat fluxes to urbanization (Figures 13a and 13b). Urban expansion increased sensible heat in the domain, and the enhanced sensible heat fluxes were dominant in the places where natural land surface was converted into impervious surface during 1990–2010. The maximum of sensible heat differences was 60 W/m^2 in these areas, while there were no significant changes in the urban cores. On the other hand, latent heat

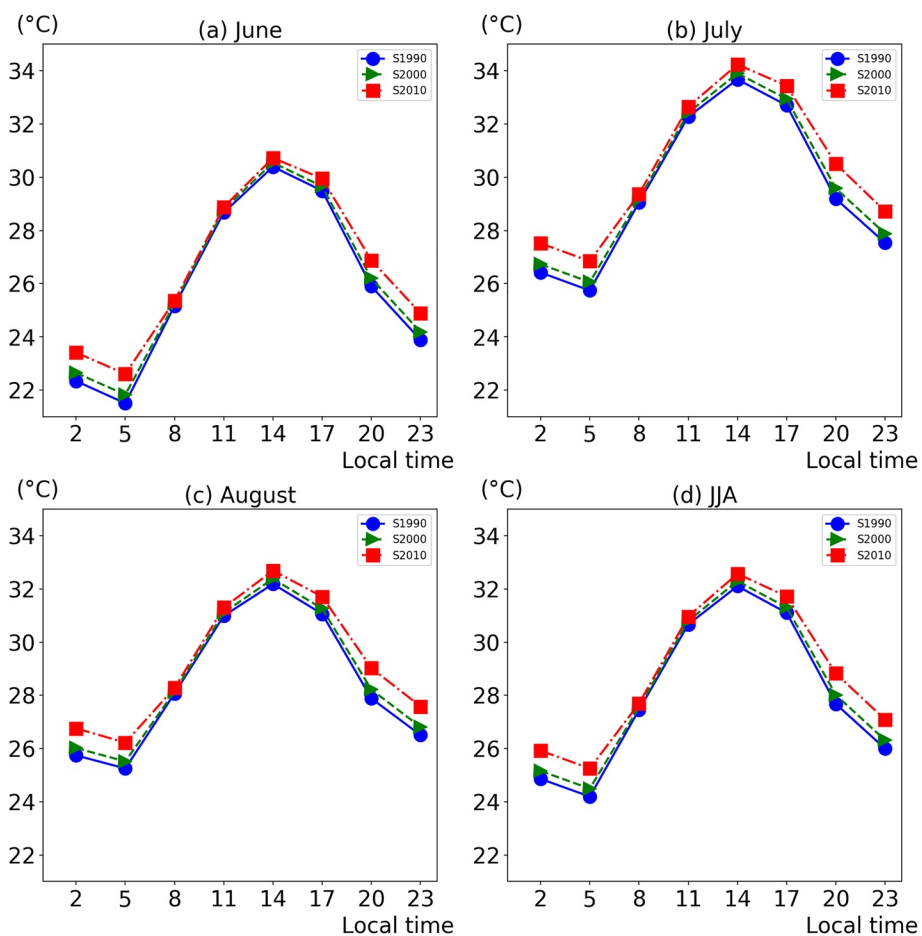


Figure 10. Diurnal cycle of simulated 2-m air temperature over urban areas in (a) June, (b) July, (c) August, and (d) Summer extracted from different Weather Research and Forecast (WRF) experiments (S1990, blue; S2000, green; S2010, red).

fluxes were reduced in urban area, and those newly built areas had the largest decrease in latent heat (up to -90 W/m^2). The differences of ground heat fluxes between S2010 and S1990 simulations were noticeably smaller compared to the sensible and latent fluxes (Figure 13c). The land surface temperature showed the largest increase ($>2^\circ\text{C}$) in the newly built area, showing a similar spatial pattern to that of the sensible heat flux (Figure 13d).

We presented the average diurnal cycles of simulated sensible heat, latent heat, ground heat, and surface temperature over the urban areas of S1990, S2000, and S2010 in Figure 14. As the cities expanded, sensible heat in urban environment increased throughout the entire day. Sensible heat differences during 1990–2010 peaked (over 100 W/m^2) at 14:00 local time. The difference was much less at night (still positive)

than in the daytime, implying more heat transferred to the atmosphere at night and raised T_{\min} . The latent heat fluxes had the largest decrease (exceeding 150 W/m^2) at 14:00 local time (Figure 14b), which resulted in great moisture loss in low-level atmosphere during the daytime. Diurnal cycle of ground heat flux showed that heat transferred from surface to subsurface in the daytime (ground flux is positive when heat is going toward the surface in Noah) and more energy was transferred into subsurface in the daytime due to urban expansion. However, the heat also transferred from subsurface to surface in nighttime when subsurface was warmer. It should be noted that the ground heat flux may be biased due to limited spin-up time (Chen et al., 2007).

Table 5
Effect Index (EI) of Urban-Induced Warming in Different Urbanization Periods

	EI values	
	1990–2000	1990–2010
T_{mean}	3.49	5.66
T_{\min}	3.27	5.75
T_{\max}	4.25	4.83

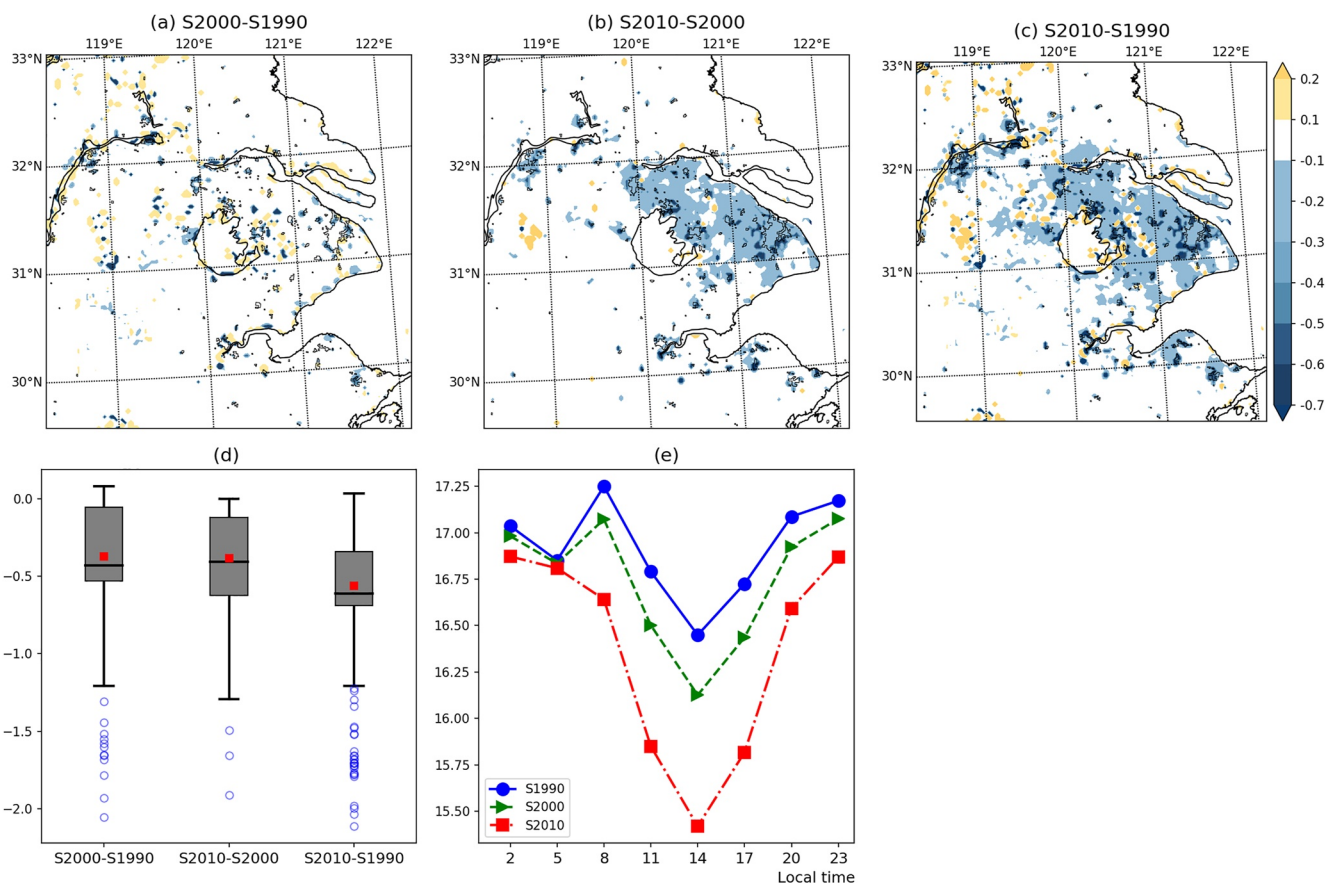


Figure 11. Changes of simulated average summer 2-m water vapor mixing ratio in grams per kilogram. Spatial map of changes derived from (a) S2000–S1990, (b) S2010–S2000, and (c) S2010–S1990. (d) Boxplot of changes over urban areas from different simulations. (e) Average diurnal cycle over urban areas in different simulations.

Although net radiation decreased slightly, a great increase in land surface temperature was observed over the study period. It was attributed to the conversion of natural land cover to urban surface. Less energy was consumed in evaporation (less latent heat fluxes and moisture in low-level atmosphere) and therefore the cooling effect was reduced. Urban land cover stored more energy and then transferred it into near-surface air through conduction and convection. Urban expansion directly affected the energy partitioning of the net radiation into sensible and latent heat fluxes. More sensible heat flux warmed the temperature of the near-surface atmosphere in urban area, producing the “urban heat island.”

4. Discussion

4.1. The Warming Effect of Historic Urbanization

Our simulations showed that urban summertime T_{mean} increased 0.75 °C due to urbanization from 1990 to 2010. Cao et al. (2016) estimated that the overall temperature increase was 0.39°C/10 years over 1990–2010 in YRD, which was consistent with our results. Lin et al. (2016) significantly underestimated the urbanization-induced warming magnitude in the region and reported the temperature increase as 0.12°C/30 years. Different configurations and spatial resolutions of simulation might be the main factors that led to the discrepancies. The 0.2° horizontal resolution in Lin's simulations was too coarse to capture the characteristics of urban land surface. Additionally, lack of two-way coupling between land surface and atmosphere in offline LSM also contributed to underestimating urban warming effect (Cao et al., 2016). In Wang et al. (2012), the warming effect was determined by calculating the difference between no-urban scenario and land cover in 2009, which substantially overestimated the temperature increase (1.74°C/20 years) in

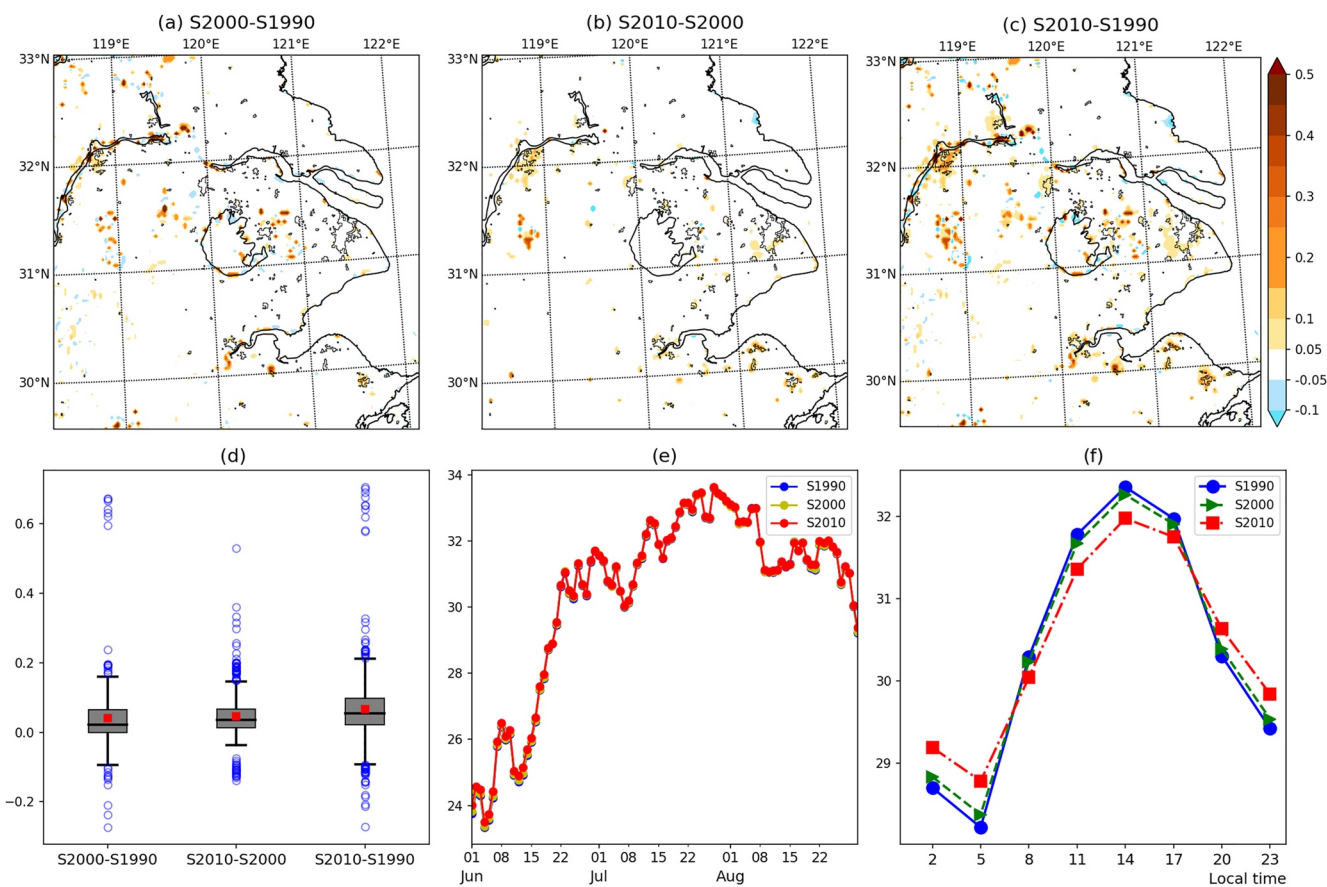


Figure 12. Change of simulated JJA heat stress index. Spatial changes derived from (a) S2000–S21990, (b) S2010–S2000, and (c) S2010–S1990. (d) Boxplot of changes over urban areas in different simulations. (e) Multiyear daily average wet-bulb globe temperature (WBGT) over urban areas in different simulations. (f) Average diurnal cycle over urban areas in different simulations.

YRD. The no-urban scenario was not even close to the land cover in the 1980s and therefore enlarged the warming magnitudes of urbanization.

Urbanization-induced warming effects derived from our simulations were supported by the analysis of urban-rural contrast. Urban area exhibited larger warming magnitude for T_{mean} than rural area (0.51 versus 0.39°C/decade) as shown in Figure 4. The contrast (0.12°C/decade) was consistent with the warming rate (0.75°C/20 years, i.e., 0.38°C/decade) in our results. It should be noted that urban-rural contrast result lies in the assumption that these rural stations were able to reflect macroscale climate change and not affected by urbanization. Nonetheless, results in Section 3.3 showed that urbanization of YRD had regionalized warming effect, and the affected region extended beyond urban environment to surrounding rural zones. Therefore, the stations in the rural areas were also affected by urbanization, and the temperature increase induced by urbanization should be greater than urban-rural contrast result (0.12 °C/decade) and less than the observed warming rate (0.51 °C/decade). These results imply that the warming rate of T_{mean} derived from our WRF simulations is more accurate.

Analysis on energy balance showed that modification of land surface during urbanization imposed substantial influences on the partitioning of net radiation into sensible and latent heat. Stronger sensible heat fluxes led to the warmer temperature in urban environment, which was consistent with the findings in previous studies conducted in YRD (Cao et al., 2016; Lin et al., 2016; Wang et al., 2012). However, the material and morphology of urban environments and local climate contributed to different warming rates between T_{max} and T_{min} . It is widely recognized that urban areas with building and other artificial materials can store extra energy during the daytime and release heat to increase T_{min} during the nighttime (Grimmond & Oke, 1999). Also, the trends in daytime temperature or T_{max} vary in different local background climates

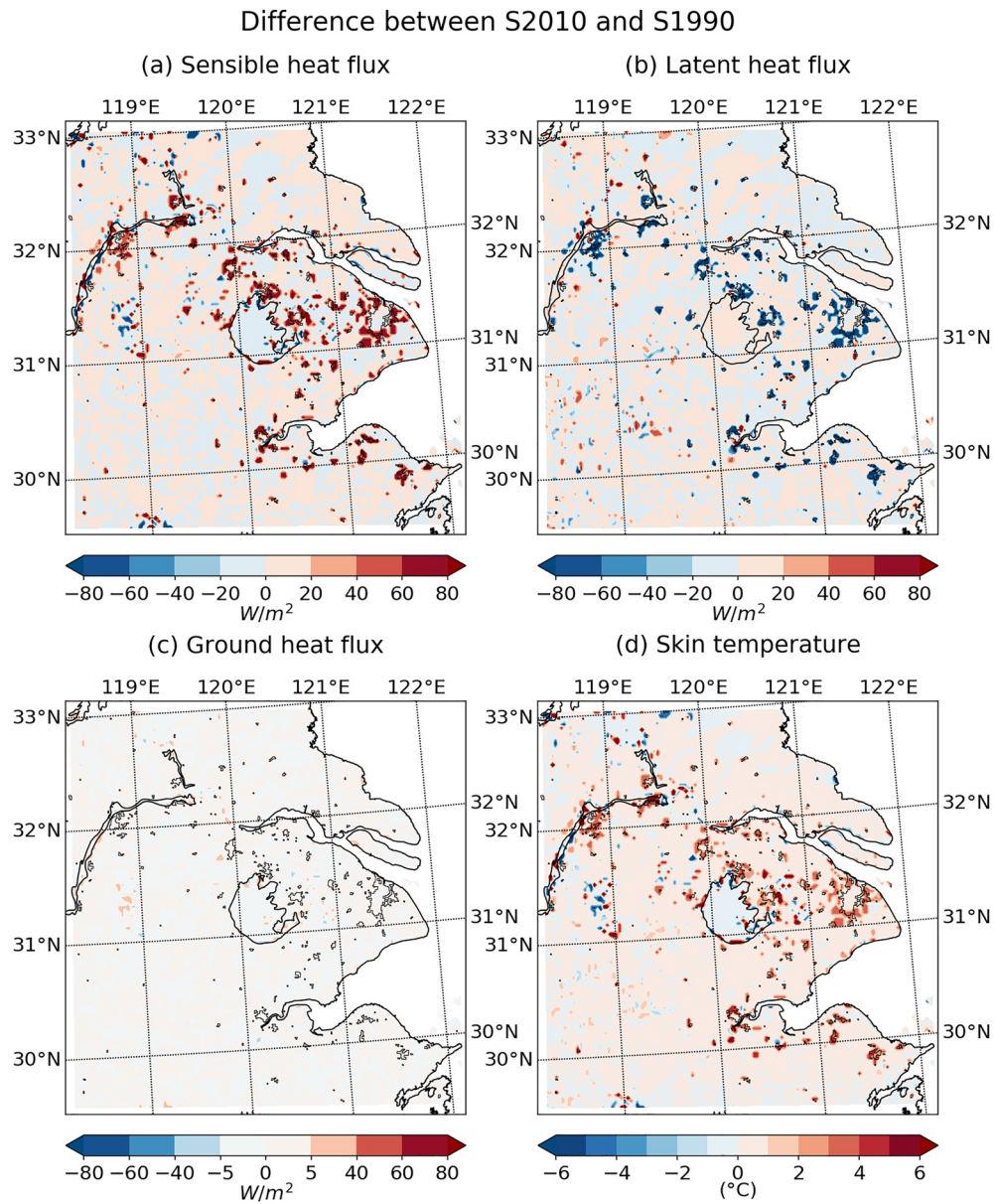


Figure 13. Spatial maps of differences in simulated (a) Sensible heat, (b) Latent heat, (c) Ground heat, and (d) Skin temperature between S2010 and S1990 experiments.

(Zhao et al., 2014). Previous studies on arid climate showed that urbanization would reduce T_{\max} and result in cool island in the daytime because of the urban structure (Georgescu, 2015; Georgescu et al., 2011). However, it is not the case in the YRD region with a humid climate. Urban expansion also induced daytime warming of near-surface air temperature in YRD, which was associated with lower heat convection efficiency in the wetter climate (Zhao et al., 2014). The warming T_{\max} reported in our experiments was consistent with previous work conducted in the YRD region (Cao et al., 2016; Zhang et al., 2010).

It is also worth noting that cooling effect was observed in some pixels as shown in Figures 7d–7f. The mean magnitude of cooling effect at these pixels was 0.13°C for T_{mean} in S2000–S1900 and became much smaller in S2010–S2000 (0.05°C). Converting a no-urban pixel (high fraction vegetation) to an urban pixel (10% vegetation) usually would not induce the cooling impact (Figure 7). We further inspected these cooling pixels and found that most of them were close to water bodies or along the coastal line, Yangtze River and lakes. We further examined the land cover changes over these pixels and found that the dominant controlling

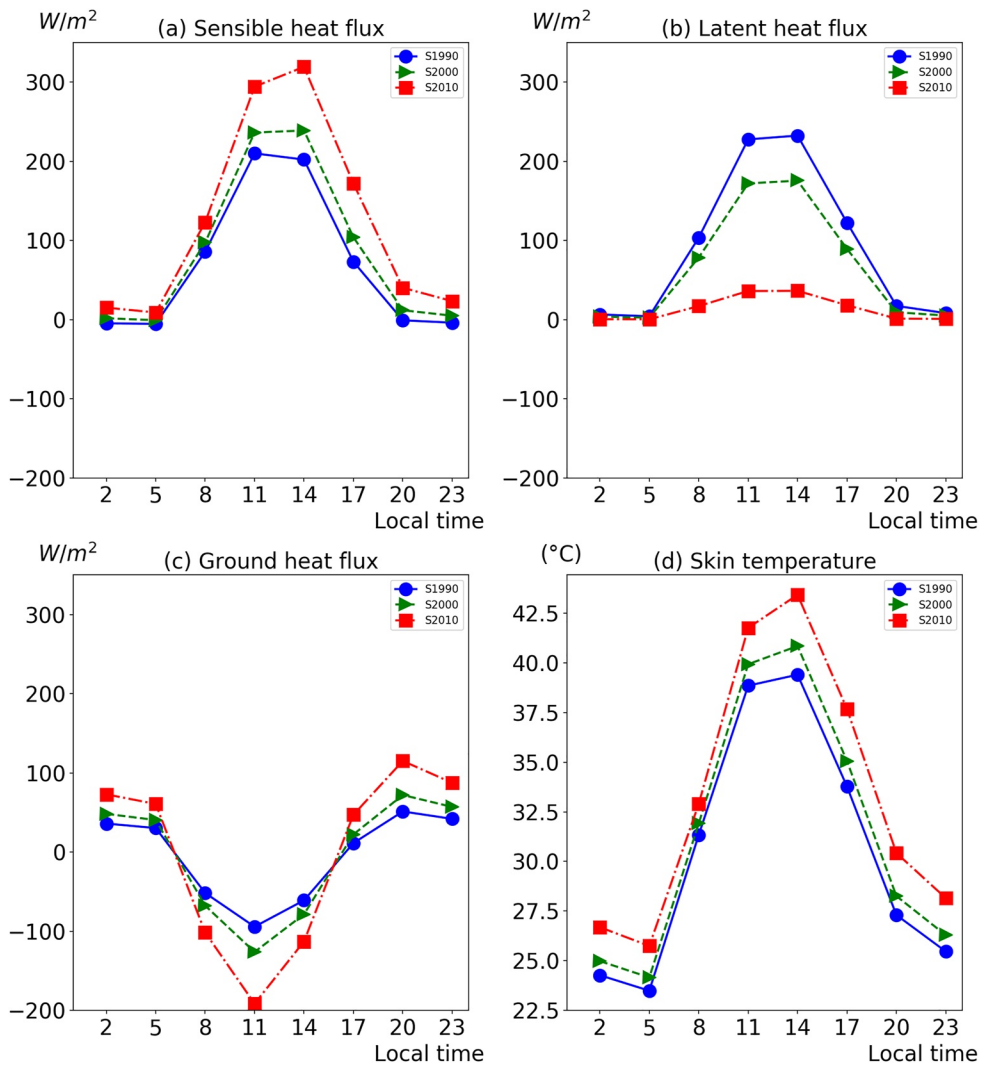


Figure 14. Average diurnal cycle of simulated JJA (a) Sensible heat, (b) Latent heat, (c) Ground heat, and (d) Skin temperature extracted from different experiments over the urban areas (S1990, blue; S2000, green; S2010, red).

factor was the conversion from natural land to water cover. This conversion caused more energy consumed during evaporation (more latent heat fluxes) and led to cooling effect of skin surface temperature in these pixels (Figure 13d). In this study, we primarily focused on temperature changes in the urban areas, and these pixels far from the cities did not impact on our major conclusions about enhanced warming effects of urban expansion.

4.2. Contributions and Limitations

We examined the warming effect of long-term urbanization in YRD by integrating historic observation and numerical modeling. A dynamic classification scheme was applied in the urban minus rural (UMR) method, and multiple historic scenarios were incorporated into WRF simulations. Both numerical simulations and observation-based analysis showed that the response of T_{\min} to urban expansion was stronger than that of T_{\max} , and warming effect was enhanced in the late stage of urbanization (after 2000). These findings imply that the enhanced warming effect on temperature in the future will exacerbate heat waves in the already heated climate. Although vapor moisture deficits in near-surface atmosphere moderately offset the increasing heat stress, continued urban expansion would pose threats on urban residents. Effective ways to

alleviate the temperature increase such as urban roof albedo management and urban landscape management should be considered in the humid regions.

The observational records at urban stations exhibited a greater temperature increase than the WRF simulation, which was due the fact that the observations were affected not only by urban land changes but other factors. Major contributors included anthropogenic heat release (AHR) and greenhouse gases (GHG) emission, and they were not considered in the numerical experiments. Good records of AHR data or related energy terms in the study domain are currently not available. Quantifying the contribution of AHR to regional climate change is also beyond the scope of this study.

The warming magnitude induced by long-term greenhouse gas (GHG) emission could be estimated from observations of stations far away from the urban cores. However, results in Section 3.3 demonstrated that the impacted areas of YRD's urbanization extended beyond urban environment to regional places. Krayenhoff et al. (2018) attempted to quantify the contribution of projected GHG-induced warming and urban expansion using the downscaled GCM (global climate models) outputs from Coupled Model Intercomparison Project (CMIP) projections. In this study, we focus on the warming effect of urban expansion in the historical period. The integrated impacts of anthropogenic heat, projected global warming, and urban expansion need further exploration and are not investigated in this study.

5. Conclusions

In this study, we examined the impacts of urban expansion on summertime temperature in the Yangtze River Delta (YRD) based on both observations and numerical modeling. The observation-based analysis showed that urbanization imposed a warming effect on urban climate over the study period, and it exerted greater influence in the late stage (after 2000). By applying WRF coupled with an urban canopy model, we estimated the urban-induced warming effect under multiple historic land use scenarios (1990, 2000, and 2010). WRF simulation showed that urban expansion during 1990–2010 caused T_{mean} , T_{min} , and T_{max} in urban area increased by 0.75°C, 1.06°C, and 0.45°C, respectively. Larger warming magnitude of T_{min} than T_{max} resulted in decrease in DTR. Both the magnitudes and the impacted areas of warming were enhanced in the late stage of urbanization. Meanwhile, Q2 was reduced by 0.56 g/kg over urban areas, resulting in intensified urban dry island (UDI) effect in the YRD. The urban-induced increase in heat stress was relatively small due to the UDI effect. Analysis of the energy balance showed that urbanization affected the energy partitioning of the net radiation into sensible and latent heat, and the increased sensible heat fluxes and reduced latent heat fluxes played a key role in temperature changes over urban areas. This study provides insights to understand urban-induced warming of near-surface atmosphere in humid urban agglomeration. In order to mitigate urban heat island effects, applying cool and green roofs (Chen & Zhang, 2018), and improving the vegetation cover ratio should be considered and further explored.

Data Availability Statement

The initial boundary conditions were provided by the National Centers for Environmental Prediction (NCEP) Global Final Analysis (FNL, <https://rda.ucar.edu/datasets/ds083.2/>). The land-use and land-cover data were from Chinese Academy of Sciences (<http://www.resdc.cn/data.aspx?DATAID=95>). The observed daily temperature data were obtained from China Meteorological Data website (<http://data.cma.cn/en>).

Acknowledgment

This work was financially supported by the National Natural Science Foundation of China (Grant 41807163, 41901026, 42177450), the Natural Science Foundation of Hunan Province (Grant 2020JJ5361, 2019JJ40188), Project of Education Department of Hunan Province (Grant 19A311), and the National Key Research and Development Program of China (Grant 2016YFC0401502).

References

- American Association for the Advancement of Science (AAAS). (2016). Rise of the city. *Science*, 352(6288), 906–907.
- Argüeso, D., Evans, J. P., Fita, L., & Bormann, K. J. (2014). Temperature response to future urbanization and climate change. *Climate Dynamics*, 42(7), 2183–2199. <https://doi.org/10.1007/s00382-013-1789-6>
- Benson-Lira, V., Georgescu, M., Kaplan, S., & Vivoni, E. R. (2016). Loss of a lake system in a megacity: The impact of urban expansion on seasonal meteorology in Mexico City. *Journal of Geophysical Research: Atmospheres*, 121, 3079–3099.
- Cao, Q., Yu, D., Georgescu, M., & Wu, J. (2016). Impacts of urbanization on summer climate in China: An assessment with coupled land-atmospheric modeling. *Journal of Geophysical Research: Atmospheres*, 121, 10505–10521. <https://doi.org/10.1002/2016JD025210>
- Cao, Q., Yu, D., Georgescu, M., Wu, J., & Wang, W. (2018). Impacts of future urban expansion on summer climate and heat-related human health in eastern China. *Environment International*, 112, 134–146. <https://doi.org/10.1016/j.envint.2017.12.027>

- Chen, F., Manning, K., LeMone, M., Trier, S., Alfieri, J., Roberts, R., et al. (2007). Description and evaluation of the characteristics of the NCAR high-resolution land data assimilation system. *Journal of Applied Meteorology and Climatology*, 46(6), 694–713. <https://doi.org/10.1175/jamc2463.1>
- Chen, F., Mitchell, K., Schaake, J., Xue, Y., Pan, H. L., Koren, V., et al. (1996). Modeling of land surface evaporation by four schemes and comparison with FIFE observations. *Journal of Geophysical Research*, 101(D3), 7251–7268. <https://doi.org/10.1029/95JD02165>
- Chen, F., Yang, X., & Zhu, W. (2014). WRF simulations of urban heat island under hot-weather synoptic conditions: The case study of Hangzhou City, China. *Atmospheric Research*, 138, 364–377. <https://doi.org/10.1016/j.atmosres.2013.12.005>
- Chen, L., & Frauenfeld, O. W. (2016). Impacts of urbanization on future climate in China. *Climate Dynamics*, 47(1), 345–357. <https://doi.org/10.1007/s00382-015-2840-6>
- Chen, Y., & Zhang, N. (2018). Urban heat island mitigation effectiveness under extreme heat conditions in the Suzhou-Wuxi-Changzhou metropolitan area, China. *Journal of Applied Meteorology and Climatology*, 57(2), 235–253. <https://doi.org/10.1175/jamc-d-17-0101.1>
- Chow, W. T. L., Brennan, D., & Brazel, A. J. (2012). Urban heat island research in phoenix, Arizona: Theoretical contributions and policy applications. *Bulletin of the American Meteorological Society*, 93(4), 517–530. <https://doi.org/10.1175/bams-d-11-00011.1>
- Cosgrove, A., & Berkelhammer, M. (2018). Downwind footprint of an urban heat island on air and lake temperatures. *npg Climate and Atmospheric Science*, 1(1), 46. <https://doi.org/10.1038/s41612-018-0055-3>
- Du, Y., Xie, Z., Zeng, Y., Shi, Y., & Wu, J. (2007). Impact of urban expansion on regional temperature change in the Yangtze River Delta. *Journal of Geographical Sciences*, 17(4), 387–398. <https://doi.org/10.1007/s11442-007-0387-0>
- Georgescu, M. (2015). Challenges associated with adaptation to future urban expansion. *Journal of Climate*, 28(7), 2544–2563. <https://doi.org/10.1175/jcli-d-14-00290.1>
- Georgescu, M., Miguez-Macho, G., Steyaert, L. T., & Weaver, C. P. (2009a). Climatic effects of 30 years of landscape change over the Greater Phoenix, Arizona, region: 1. Surface energy budget changes. *Journal of Geophysical Research*, 114, D05110. <https://doi.org/10.1029/2008JD010745>
- Georgescu, M., Miguez-Macho, G., Steyaert, L. T., & Weaver, C. P. (2009b). Climatic effects of 30 years of landscape change over the Greater Phoenix, Arizona, region: 2. Dynamical and thermodynamical response. *Journal of Geophysical Research*, 114, D05111. <https://doi.org/10.1029/2008JD010762>
- Georgescu, M., Moustaqui, M., Mahalov, A., & Dudhia, J. (2011). An alternative explanation of the semiarid urban area “oasis effect”. *Journal of Geophysical Research*, 116, D24113. <https://doi.org/10.1029/2011JD016720>
- Georgescu, M., Moustaqui, M., Mahalov, A., & Dudhia, J. (2013). Summer-time climate impacts of projected megapolitan expansion in Arizona. *Nature Climate Change*, 3(1), 37–41. <https://doi.org/10.1038/nclimate1656>
- Grimm, N. B., Faeth, S. H., Golubiewski, N. E., Redman, C. L., Wu, J., Bai, X., & Briggs, J. M. (2008). Global change and the ecology of cities. *Science*, 319(5864), 756–760. <https://doi.org/10.1126/science.1150195>
- Grimmond, C. S. B., & Oke, T. R. (1999). Heat storage in urban areas: Local-scale observations and evaluation of a simple model. *Journal of Applied Meteorology*, 38(7), 922–940. [https://doi.org/10.1175/1520-0450\(1999\)038<922:hsiu1>2.0.co;2](https://doi.org/10.1175/1520-0450(1999)038<922:hsiu1>2.0.co;2)
- Hao, L., Huang, X., Qin, M., Liu, Y., Li, W., & Sun, G. (2018). Ecohydrological processes explain urban dry island effects in a wet region, Southern China. *Water Resources Research*, 54, 6757–6771. <https://doi.org/10.1029/2018WR023002>
- Heaviside, C., Cai, X. M., & Vardoulakis, S. (2015). The effects of horizontal advection on the urban heat island in Birmingham and the West Midlands, United Kingdom during a heatwave. *Quarterly Journal of the Royal Meteorological Society*, 141(689), 1429–1441. <https://doi.org/10.1002/qj.2452>
- Howard, L. (1833). The climate of London (Vol. 1, p. 348). Harvey and Darton.
- Hua, L., Ma, Z., & Guo, W. (2008). The impact of urbanization on air temperature across China. *Theoretical and Applied Climatology*, 93(3), 179–194. <https://doi.org/10.1007/s00704-007-0339-8>
- Kalnay, E., & Cai, M. (2003). Impact of urbanization and land-use change on climate. *Nature*, 423(6939), 528–531. <https://doi.org/10.1038/nature01675>
- Ke, X., Wu, F., & Ma, C. (2013). Scenario analysis on climate change impacts of urban land expansion under different urbanization patterns: A case study of Wuhan metropolitan. *Advances in Meteorology*, 293636. <https://doi.org/10.1155/2013/293636>
- Kong, D., Gu, X., Li, J., Ren, G., & Liu, J. (2020). Contributions of global warming and urbanization to the intensification of human-perceived heatwaves over China. *Journal of Geophysical Research: Atmospheres*, 125, e2019JD032175. <https://doi.org/10.1029/2019JD032175>
- Krayenhoff, E. S., Moustaqui, M., Broadbent, A. M., Gupta, V., & Georgescu, M. (2018). Diurnal interaction between urban expansion, climate change and adaptation in US cities. *Nature Climate Change*, 8(12), 1097–1103. <https://doi.org/10.1038/s41558-018-0320-9>
- Kusaka, H., & Kimura, F. (2004). Coupling a Single-Layer Urban Canopy Model with a simple atmospheric model: Impact on urban heat island simulation for an idealized case. *Journal of the Meteorological Society of Japan. Series II*, 82(1), 67–80. <https://doi.org/10.2151/jmsj.82.67>
- Liao, J., Wang, T., Wang, X., Xie, M., Jiang, Z., Huang, X., & Zhu, J. (2014). Impacts of different urban canopy schemes in WRF/Chem on regional climate and air quality in Yangtze River Delta, China. *Atmospheric Research*, 145–146, 226–243. <https://doi.org/10.1016/j.atmosres.2014.04.005>
- Liao, W., Liu, X., Li, D., Luo, M., Wang, D., Wang, S., et al. (2018). Stronger contributions of urbanization to heat wave trends in wet climates. *Geophysical Research Letters*, 45, 11310–11317. <https://doi.org/10.1029/2018GL079679>
- Lin, L., Ge, E., Liu, X., Liao, W., & Luo, M. (2018). Urbanization effects on heat waves in Fujian province, Southeast China. *Atmospheric Research*, 210, 123–132. <https://doi.org/10.1016/j.atmosres.2018.04.011>
- Lin, S., Feng, J., Wang, J., & Hu, Y. (2016). Modeling the contribution of long-term urbanization to temperature increase in three extensive urban agglomerations in China. *Journal of Geophysical Research: Atmospheres*, 121, 1683–1697. <https://doi.org/10.1002/2015JD024227>
- Liu, J. Y., Kuang, W. H., Zhang, Z. X., Xu, X. L., Qin, Y. W., Ning, J., et al. (2014). Spatiotemporal characteristics, patterns, and causes of land-use changes in China since the late 1980s. *Journal of Geographical Sciences*, 24(2), 195–210. <https://doi.org/10.1007/s11442-014-1082-6>
- Luo, M., & Lau, N.-C. (2019). Urban expansion and drying climate in an urban agglomeration of East China. *Geophysical Research Letters*, 46, 6868–6877. <https://doi.org/10.1029/2019GL082736>
- McDonald, R. I., Green, P., Balk, D., Fekete, B. M., Revenga, C., Todd, M., & Montgomery, M. (2011). Urban growth, climate change, and freshwater availability. *Proceedings of the National Academy of Sciences of the United States of America*, 108(15), 6312–6317. <https://doi.org/10.1073/pnas.1011615108>
- Miao, S., Chen, F., LeMone, M. A., Tewari, M., Li, Q., & Wang, Y. (2009). An observational and modeling study of characteristics of urban heat island and boundary layer structures in Beijing. *Journal of Applied Meteorology and Climatology*, 48(3), 484–501. <https://doi.org/10.1175/2008jamc1909.1>

- Ren, G., Zhou, Y., Chu, Z., Zhou, J., Zhang, A., Guo, J., & Liu, X. (2008). Urbanization effects on observed surface air temperature trends in North China. *Journal of Climate*, 21(6), 1333–1348. <https://doi.org/10.1175/2007jcli1348.1>
- Skamarock, W. C., Klemp, J. B., Dudhia, J., Gill, D. O., Barker, D., Duda, M. G., & Powers, J. G. (2008). *A description of the Advanced Research WRF version 3 (No. NCAR/TN-475+STR)*. University Corporation for Atmospheric Research. <https://doi.org/10.5065/D68S4MVH>
- Thompson, R. D., & Perry, A. H. (1997). *Applied climatology: Principles and practice*. Psychology Press.
- Wang, J., Feng, J., & Yan, Z. (2015). Potential sensitivity of warm season precipitation to urbanization extents: Modeling study in Beijing-Tianjin-Hebei urban agglomeration in China. *Journal of Geophysical Research: Atmospheres*, 120, 9408–9425. <https://doi.org/10.1002/2015JD023572>
- Wang, J., Feng, J., Yan, Z., Hu, Y., & Jia, G. (2012). Nested high-resolution modeling of the impact of urbanization on regional climate in three vast urban agglomerations in China. *Journal of Geophysical Research*, 117, D21103. <https://doi.org/10.1029/2012JD018226>
- Wang, M., Zhang, X., & Yan, X. (2013). Modeling the climatic effects of urbanization in the Beijing-Tianjin-Hebei metropolitan area. *Theoretical and Applied Climatology*, 113(3–4), 377–385. <https://doi.org/10.1007/s00704-012-0790-z>
- Wang, X., Liao, J., Zhang, J., Shen, C., Chen, W., Xia, B., & Wang, T. (2014). A numeric study of regional climate change induced by urban expansion in the Pearl River Delta, China. *Journal of Applied Meteorology and Climatology*, 53(2), 346–362. <https://doi.org/10.1175/jamc-d-13-054.1>
- Willett, K. M., & Sherwood, S. C. (2012). Exceedance of heat index thresholds for 15 regions under a warming climate using the wet-bulb globe temperature. *International Journal of Climatology*, 32(2), 161–177. <https://doi.org/10.1002/joc.2257>
- Xiao, P., Wang, X., Feng, X., Zhang, X., & Yang, Y. (2014). Detecting China's urban expansion over the past three decades using nighttime light data. *IEEE Journal of Selected Topics in Applied Earth Observations and Remote Sensing*, 7(10), 4095–4106. <https://doi.org/10.1109/jstars.2014.2302855>
- Yang, B., Zhang, Y., & Qian, Y. (2012). Simulation of urban climate with high-resolution WRF model: A case study in Nanjing, China. *Asia-Pacific Journal of Atmospheric Sciences*, 48(3), 227–241. <https://doi.org/10.1007/s13143-012-0023-5>
- Yang, L., Niyogi, D., Tewari, M., Aliaga, D., Chen, F., Tian, F., & Ni, G. (2016). Contrasting impacts of urban forms on the future thermal environment: Example of Beijing metropolitan area. *Environmental Research Letters*, 11(3), 034018. <https://doi.org/10.1088/1748-9326/11/3/034018>
- Yang, L., Tian, F., Smith, J. A., & Hu, H. (2014). Urban signatures in the spatial clustering of summer heavy rainfall events over the Beijing metropolitan region. *Journal of Geophysical Research: Atmospheres*, 119, 1203–1217. <https://doi.org/10.1002/2013JD020762>
- Yang, X., Hou, Y., & Chen, B. (2011). Observed surface warming induced by urbanization in east China. *Journal of Geophysical Research*, 116, D14113. <https://doi.org/10.1029/2010JD015452>
- Yang, X., Ruby Leung, L., Zhao, N., Zhao, C., Qian, Y., Hu, K., et al. (2017). Contribution of urbanization to the increase of extreme heat events in an urban agglomeration in east China. *Geophysical Research Letters*, 44, 6940–6950. <https://doi.org/10.1002/2017GL074084>
- Zhang, N., Gao, Z., Wang, X., & Chen, Y. (2010). Modeling the impact of urbanization on the local and regional climate in Yangtze River Delta, China. *Theoretical and Applied Climatology*, 102(3), 331–342. <https://doi.org/10.1007/s00704-010-0263-1>
- Zhao, L., Lee, X., Smith, R. B., & Oleson, K. (2014). Strong contributions of local background climate to urban heat islands. *Nature*, 511(7508), 216–219. <https://doi.org/10.1038/nature13462>
- Zhou, L., Dickinson, R. E., Tian, Y., Fang, J., Li, Q., Kaufmann, R. K., et al. (2004). Evidence for a significant urbanization effect on climate in China. *Proceedings of the National Academy of Sciences of the United States of America*, 101(26), 9540–9544. <https://doi.org/10.1073/pnas.0400357101>